XXV INTERNATIONAL SYMPOSIUM
========
"NANOSTRUCTURES: PHYSICS AND TECHNOLOGY",
========
SAINT PETERSBURG, RUSSIA, JUNE 26–30, 2017.

NANOSTRUCTURE TECHNOLOGY

Effect of Epitaxial Alignment on Electron Transport from Quasi-Two-Dimensional Iron Silicide α-FeSi$_2$ Nanocrystals Into p-Si(001)[1]

I. A. Tarasov*, M. V. Rautskii, I. A. Yakovlev, and M. N. Volochaev

Kirensky Institute of Physics, Federal Research Centre KSC SB RAS, Krasnoyarsk, 660036 Russia
*e-mail: tia@iph.krasn.ru
Received December 25, 2017

Abstract—Self-assembled growth of α-FeSi$_2$ nanocrystal ensembles on gold-activated and gold-free Si(001) surface by molecular beam epitaxy is reported. The microstructure and basic orientation relationship (OR) between the silicide nanocrystals and silicon substrate were analysed. The study reveals that utilisation of the gold as catalyst regulates the preferable OR of the nanocrystals with silicon and their habitus. It is shown that electron transport from α-FeSi$_2$ phase into p-Si(001) can be tuned by the formation of (001)—or (111)—textured α-FeSi$_2$ nanocrystals ensembles. A current-voltage characteristic of the structures with different preferable epitaxial alignment (α-FeSi$_2$(001)/Si(100) and α-FeSi$_2$(111)/Si(100)) shows good linearity at room temperature. However, it becomes non-linear at different temperatures for different ORs due to different Schottky barrier height governed by a particular epitaxial alignment of the α-FeSi$_2$/p-Si interfaces.

INTRODUCTION

With the development of the conventional silicon CMOS technology, the typical device continues to decrease while the problem of parasitic resistance becomes very significant causing a limitation of the nanoscale semiconductor device performance [1, 2]. Parasitic resistance is largely dominated by contact resistance. To decrease specific contact resistance of metal/semiconductor junction, control and tunning of the Schottky barrier height φ_{B_0} is needed. In real metal/semiconductor contact the metal Fermi level is pinned near the charge neutrality level forming Schottky barrier for electrons and holes. Metal electron wave functions penetrate into semiconductor band gap creating metal induced gap states [3] causing a dipole charge formation. The system tends to minimise this dipole charge aligning the position of the metal Fermi level and the charge neutrality level. This metal Fermi level pinning is determined by the semiconductor's dielectric screening (pinning factor S) [4]. Usually this value is lower for semiconductors than in oxide and other dielectrics, where the phenomenon of Fermi level pinning does not exist. As it is reported, there are methods to reduce the contact resistance in metal-semiconductor junction. First is an increase of

the electrically active dopant density in semiconductor, the second one—to create an additional dipole at the M–S interface to modulate the barrier height, the third one—de-pinning the Schottky barrier height by inserting thin dielectric layer with high S factor. While first method is effective for n-Si to thin the barrier allowing sufficient value of tunneling current, it is not suitable in the case of p-Si due to not enough electrical activation of dopants. Therefore, the creation of additional dipole or the Fermi level de-pinning are more suitable for tuning contact resistance in metal/p-Si junctions. Dipole manipulation is usually reached by implantation of neutral Ge or C into silicon. However the dipole charge formation caused by penetration metal electron function can also be adjust with tuning of metal contact layer epitaxial alignment, where the metal demonstrates anisotropy of electron wave function due to epitaxial strain or its crystal structure. Widely used for interconnection metal silicides can produce effective barrier heights around ~0.2 eV [1] and their capabilities still have a big prospective for further development of the nanoscale contacts. Iron silicides-based nanostructures have a wide spectrum of possible industrial application in the different fields [5]. Mainly, interest to these functional materials is caused by their ecological safety and Earth's core abundance that give us opportunity for greener future with highly effective electronic devices. Thus, metallic

---

[1]The article is published in the original.

iron silicide α-FeSi$_2$ is reported to apply as an electrode material to silicon or β-FeSi$_2$ with good ohmic characteristics [6, 7]. This phase could also be used for formation of Schottky barrier contacts, gate electrodes, local interconnects, and diffusion barriers. Its quasi-two-dimensional crystal structure gives opportunity to control electron transport from this phase into a semiconductor through variation of the epitaxial alignment on silicon.

The α-FeSi$_2$ phase belongs to tetragonal crystal system (P4mmm) with lattice parameters a, b = 2.684 Å, c = 5.128 Å [8], where Fe atoms form quasi-two-dimensional structure and are located in $\alpha\{001\}$ planes separated by two Si atom formed sheets. Thus, one can expect a higher conductance in $\{100\}$ in comparison with perpendicular [001] direction. Paramagnetic and metastable in bulk conditions α-FeSi$_2$ phase [9] at nanoscale appear to show ferromagnetic properties with magnetisation higher than the pure iron has [10−12]. Along with this, it is believed that such quasi-two-dimensional compounds as α-FeSi$_2$ may reveal high-temperature superconductivity [9]. However, despite structural similarities of α-FeSi$_2$ with pnictides and chalcogenides proper structural and electronic criteria have to be fulfilled to reach superconductivity phenomenon [9]. Hence, α-FeSi$_2$ appears as a material with the interesting properties that can be tuned by specific chemical order or stresses in α-FeSi$_2$ nanostructures [13, 14]. To date, forming the epitaxial α-FeSi$_2$ thin film via pulsed laser deposition [14], annealing of prior deposited Fe film [15, 16], ion implantation [17], polycrystalline film via facing target radio-frequency magnetron sputtering method [18], and subsequent Fe deposited layer annealing [19] were reported. Self-assembled α-FeSi$_2$ nanocrystals were synthesized on Si(001), and Si(111) surfaces by ion implantation [20], solid-phase epitaxy [10], and microwave plasma assisted chemical vapour deposition [7]. It was reported that endotaxial α-FeSi$_2$ NWs are grown by deposition Fe on Si(110) at 650°C [21], whereas under similar conditions (600 and 700°C) the growth of s-FeSi$_2$ and γ-FeSi$_2$ phases were reported, respectively [22, 23]. Despite the fact that α-FeSi$_2$ is considered to be a metastable phase in bulk, below 915−960°C it transforms into β-FeSi$_2$ phase according to the eutectoid reaction α-FeSi$_2$ → β-FeSi$_2$ + Si [24], several reports about crystal structure and physical properties of single bulk crystal and polycrystalline samples exist. The comprehensive study of well-defined α-FeSi$_2$ single crystal has been recently carried out [9]. Moreover, α-FeSi$_2$ phase and Fe rich alloy phases with DO3, B2, A2 crystal structures [25] can coexist under different growth conditions [5, 26]. Therefore, this may result in unambiguous phase identification and contradictory results reported in literature available. Thus, here we report an approach to change the epitaxial alignment of α-FeSi$_2$ phase grown on Si(001) and also carry out preliminary examination its effect on the electron transport in hybrid nanostructures α-FeSi$_2$/p-Si.

1. EXPERIMENT

The α-FeSi$_2$ nanocrystals were formed on 1°-miscut vicinal p-Si (100) substrate (ρ ~ 5−10 Ω cm, n = 2 × 10^{15} cm^{-3}) at 840°C by molecular beam epitaxy (MBE) in ultrahigh vacuum conditions (UHV) in Angara chamber [27]. Before growth, Si substrate was chemically cleaned by the technique described [28]. Si substrate was exposed to a gradual thermal treatment for 3 hours to 650°C at the rate of 4°C/min in UHV (base pressure 6.5 × 10^{-8} Pa). To obtain an atomically clean silicon surface, the wafer was flashed at 850−900°C until well-ordered (2 × 1) reconstruction appeared in the reflection high-energy electron diffraction pattern. After the specimen was cooled down to room temperature Au layer (1 nm) was evaporated from Knudsen effusion cell onto substrate surface at rate 0.25 nm/min. Then the substrate temperature was increased to 840°C, and Fe and Si were deposited simultaneously with the growth rates of 0.22 and 0.13 nm/min (AS sample) during 60 min. To highlight the influence of Au island layer on the growth of FeSi$_2$ nanostructures the following samples marked with S were prepared by the same procedure but without the Au layer deposition. Ex situ determination of the morphology, phase composition of the sample was performed by transmission electron microscopy on Hitachi HT7700 microscope equipped with ED spectrometer 6T/60 Bruker and X-ray diffraction (XRD) analysis on a PANalytical X'Pert PRO diffractometer equipped with a solid state detector PIXcel on Cu Ka radiation. Transport properties were examined with the help of cryogenic probe station Lakeshore EMPX-HF 2 and homebuilt facility [29] based on a helium cryostat and KEITHLEY-2634 current/voltage source meter in the temperature range from 4.2 K to 300 K.

2. RESULTS AND DISCUSSION

XRD patterns of the samples (Fig. 1) reveal six basic orientations of α-FeSi$_2$ crystallites on the Si(100) substrate: 001, 111, 110, 102, 211, and 100. The sample S2 is almost mono-oriented with (111) planes parallel to Si(100). From the asymmetric φ-scans (not shown here), the following epitaxial orientations have been determined: α-FeSi$_2$(001)[110] ∥ Si(001)[110], α-FeSi$_2$(001)[110] ∥ Si(001)[100] and α-FeSi$_2$(111)[−110] ∥ Si(001)[110]. The α-FeSi$_2$ lattice parameters and fractions of crystallites of different orientations in the samples (Table 1) were determined by the full-profile refinement of the symmetric and offset diffraction

scans using the derivative difference minimisation method [30].

Thus, we distinguish and pick out over the AS and S samples several orientation relationships OR of the α-FeSi$_2$ nanocrystals, where epitaxial alignment on $\alpha(001)$ plane and $\alpha(111)$ are preferable for the AS and S sample. As a result, one could expect the appearance of noticeable effect on electron transport into p-Si(001) caused by the different alignment of high-conductance channels in α-FeSi$_2$. In case of α-FeSi$_2$(001)[110] $\|$ Si(001)[110], α-FeSi$_2$(001)[110] $\|$ Si(001)[100] orientation relationships OR such channels are mainly located parallel to the Si(001) plane and electron transport will chiefly determined by electron movement in α[001] direction (Fig. 2a). Whereas in case of the α-FeSi$_2$(111)[−110] $\|$ Si(001)[110] OR the high conductance channels are located at angle of 69° to Si(001) and the main impact into the electron transport will be due to electron movement in $\alpha\langle100\rangle$ directions (Fig. 2b). While α-FeSi$_2$ nanocrystals are well separated from each other, the α/Si hybrid structures represent two Schottky diodes connected in opposite to each other through the silicon volume. The junction of metallic α-FeSi$_2$ with silicon forms the Schottky diode. Current contacts are made from indium. Inset of the Fig. 3b draws a schematic illustration of the device utilised for the measurements and its circuit diagram. One can easily see that the resistance temperature dependencies are identical for both samples and decrease with the temperature decrease, down to 220 K. This indicates that the α/Si structure resistance is determined by the resistance temperature dependence of the silicon substrate R_{Si}. In case of doped silicon, the resistance decrease is caused by an increase in the charge carrier mobility with the temperature decrement in the range from 270 down to 220 K.

Moreover, the current-voltage characteristics obtained for both samples AS (preferable OR on $\alpha(001)$) and S (preferable OR on $\alpha(111)$) at 273 K (Fig. 3b) showed good linearity, which allows one to conclude that the Schottky barrier height is very small or negative, or the semiconductor contact region is heavily doped, i.e., the α-FeSi$_2$ nanocrystals form an Ohmic contact with the silicon substrate. According to the TEM images, the α-FeSi$_2$ nanocrystals in both preferable ORs cases have a sharp interface, and one can not expect a formation of a highly-doped interlayer between the α-FeSi$_2$ nanocrystals and silicon. Therefore, Ohmic contact presence between α-FeSi$_2$ and silicon is due to low hight of the Schottky barrier.

While the temperature drops down Fermi level inside the band gap of p-doped silicon moves to valence band and as a result, the Schottky barrier height increases. Consequently, this entails a resis-
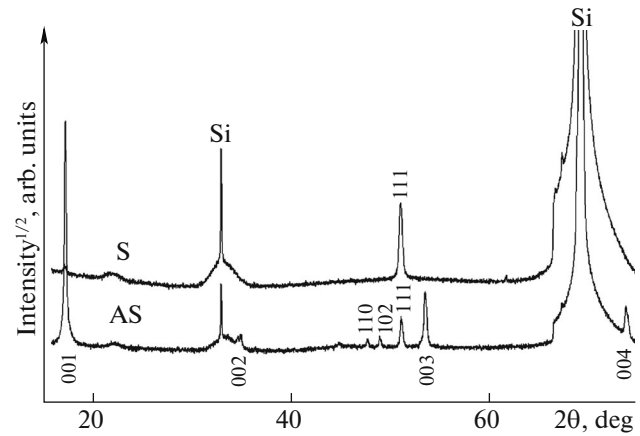
Fig. 1. XRD patterns of the samples (1) AS, (2) S Reflection indexes are marked.

tance increase. However, the resistance behaves differently (Fig. 3a) for the samples with the different preferable OR. The current-voltage characteristics at 230 K for the sample S (preferable OR on $\alpha(111)$) is still linear, whereas the sample AS (preferable OR on α (001)) shows a clear deviation from the linear dependence of the current-voltage characteristic (Fig. 3c). The current-voltage characteristic of the sample S becomes non-linear with further temperature decrease (Figs. 3a, 3c inset). Since the structures examined represent two Schottky diodes connected in opposite to each other, then the resistance of such structure is determined by reverse bias branch of the Schottky diode independently on the sign of the voltage applied. The current through the ideal diode with reverse bias is determined by the formula:

$$J_R \simeq J_s \left(\text{for} V_R > \frac{3kT}{q} \right)$$
$$= A^{**} T^2 \exp\left(-\frac{q\varphi_{B_0}}{kT} \right) \times \exp\left(+q\sqrt{\frac{q\mathscr{E}}{4\pi\varepsilon_{Si}}}/kT \right), \quad (1)$$

Table 1. FeSi$_2$ lattice parameters and fractions of crystallites of different orientations

Sample	AS	S
Lattice parameters, Å		
a	2.6948(2)	2.6967(4)
c	5.1352(2)	5.136(2)
Fractions of orientations, %		
FeSi$_2$(001) $\|$ Si(001)	69.2	0.3
FeSi$_2$(111) $\|$ Si(001)	25.0	99
FeSi$_2$(110) $\|$ Si(001)	0.8	—
FeSi$_2$(102) $\|$ Si(001)	5.1	—
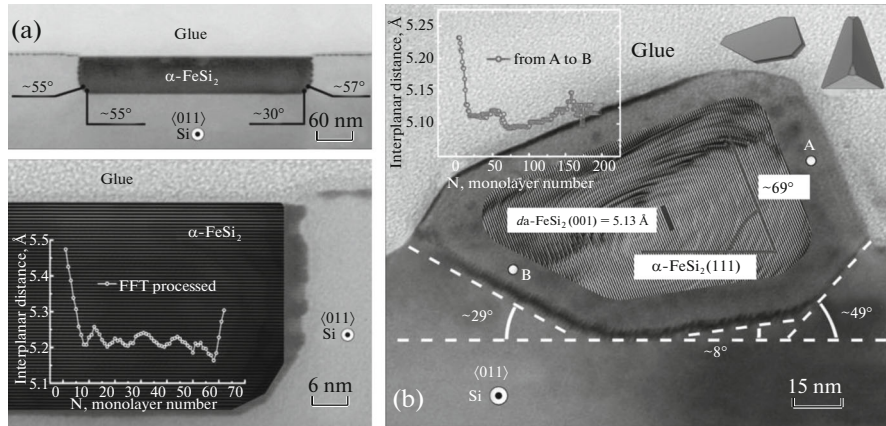
Fig. 2. Transmission electron microscopy images for typical nanocrystal with α-FeSi$_2$(001)[110] ∥ Si(001)[110] or α-FeSi$_2$(001)[110] ∥ Si(001)[100] OR (a) and α-FeSi$_2$(001)[110] ∥ Si(001)[100] (b).
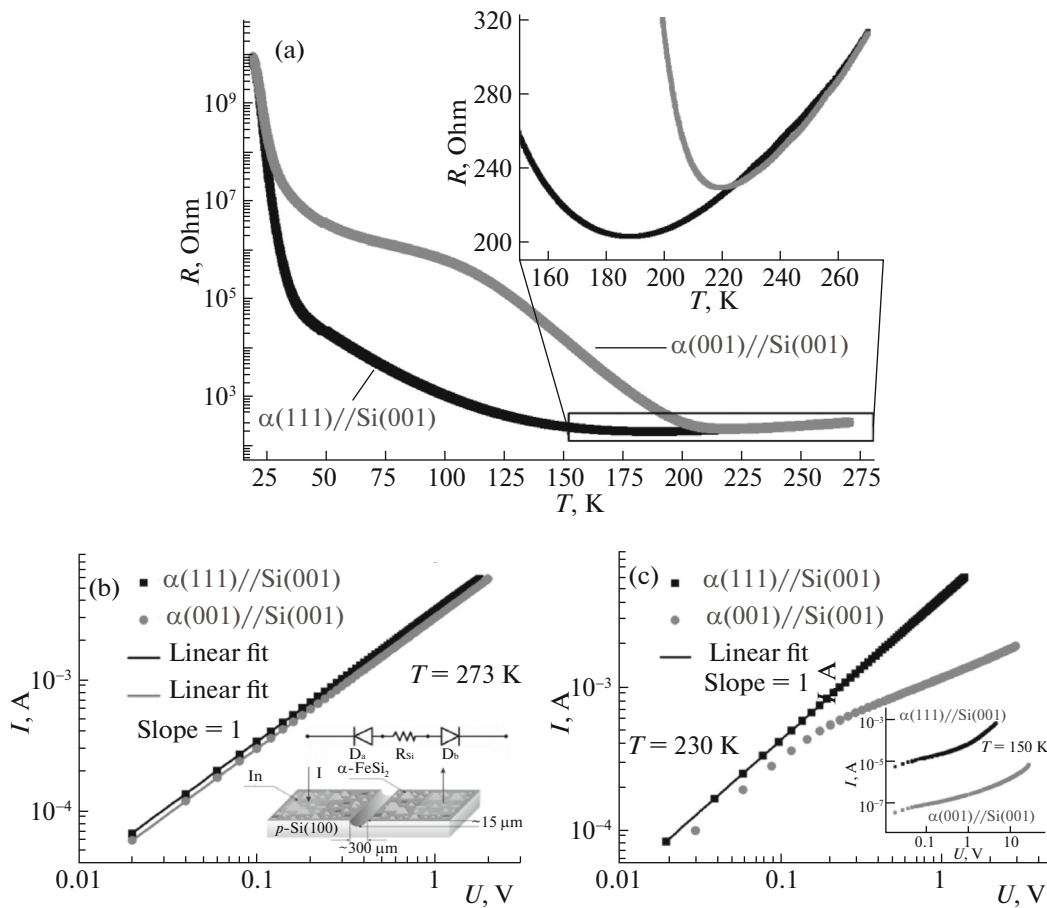
Fig. 3. (a) Temperature dependence of the α-FeSi$_2$/Si hybrid structures resistance with different preferable OR, on α(001) and α(111) planes, inset demonstrates a magnified view of the dependencies. Current-voltage characteristics of α-FeSi$_2$/Si structures at 273 K (b), 230 K (c) and 150 K (c inset). Schematic illustration of the device utilised for measurements along with its circuit diagram (b inset).

where $\mathcal{E} = \sqrt{\dfrac{2qN_D}{\varepsilon_{Si}}\left(V + V_{bi} - \dfrac{kT}{q}\right)}$, q is electron charge, φ_{B_0} is the zero-field asymptotic barrier height, A^{**} is the effective Richardson constant, k is Boltzman's constant, T is temperature, N_D is donor concentration, ε_s is permitivity of silcon [31]. When the barrier height $q\varphi_{Bn}$ is greatly lower than the bandgap the current caused by generation-recombination processes is

small in comparison with the emission current through the barrier. In this case, the reverse current increases with the voltage raise according to the expression (1). The expression (1) indicates that the difference in the α/Si structure resistance can be caused by different Schottky barrier height. However, the main impact to the reverse bias in majority of the Schottky diodes utilised in applications is contributed by the electric field concentration in the metallic electrode edge and are analogous to the currents in $p{-}n$ junctions with small curvature radius.

At the temperature 150 K, the Js of the structures differ by two orders of magnitude (Fig. 3c inset). Since the edge effects increase the reverse current, the AS sample resistance should be smaller than in case of the sample S due to the average crystallite size of the AS sample is smaller than for the S sample. Apparently, the temperature dependence different behaviour of the α/Si structure is governed by the other reason. As an origin of the effect observed one could suggest that electron wave functions of α-FeSi$_2$ silicide penetrate into the silicon bandgap in a different way for the different type of the α/Si interface. This quantum mechanical effect results in the formation of a static dipole field on the interface surface. A change in the barrier height determined by this dipole field depends on the voltage applied (i.e., on $\partial\varphi_{BO}/\partial\mathscr{E}_m \neq 0$) and as first the assumption can be represented as

$$(\Delta\varphi)_{\text{stat.}} \simeq \alpha\mathscr{E}_m, \tag{2}$$

where $\alpha \equiv \partial\varphi_{BO}/\partial\mathscr{E}_m$ [31]. It is possible in our case that namely the difference in preferable OR of the α-FeSi$_2$ crystallites and its quasi two-dimensional crystal structure are responsible for difference in the α/Si structure resistance. One can suggest that the mobility of electrons and as a result the conductance along the α(001) planes ({100} directions) formed by iron atoms in α-FeSi$_2$ should be higher than in perpendicular direction [001]. Thus, the electron wave functions of the α-FeSi$_2$ crystallites with preferable OR on α(111) plane can penetrate the silicon band gap deeper than those ones for α-FeSi$_2$ crystallites with preferable OR on α(001) plane. In turn, this can result in noticeable decrease of the Schottky barrier height for S2 (preferable OR on α(111)) in comparison with the sample AS (preferable OR on α(001)).

CONCLUSIONS

In summary, the growth of α-FeSi$_2$ nanocrystals on Si (100) by molecular beam epitaxy in presence and absence of Au catalyst is reported. The microstructure and orientation relationships of α/Si interfaces formed are determined. It was shown that the deposition of the Fe and Si with Fe-enriched stoichiometry (3:1) onto with Au-activated and non-activated Si(001) surface at 840°C results in formation α-FeSi$_2$ free-standing epitaxial nanocrystals with different preferable OR. The α-FeSi$_2$(001)//Si(001) OR was appeared to be for gold-activated Si(001) surface. Whereas the absence of the Au catalyst strongly affects the morphology and the preferable OR of the α-FeSi$_2$/Si system so that the α-FeSi$_2$ phase is formed as a highly-textured nanocrystal ensemble with texture on α-FeSi$_2$ (111) plane. It was shown that, in certain conditions, electron transport from α-FeSi$_2$ phase can be tuned by the formation of (001)—or (111)—textured α-FeSi$_2$ nanocrystal ensembles. A current-voltage characteristic of the structures with both preferable ORs, α-FeSi$_2$(001)/Si(100) and α-FeSi$_2$(111)/Si(100), showed good linearity at room temperature. However, it changes to non-linear behaviour at different temperatures due to different Schottky barrier height governed by the particular epitaxial alignment of the α-FeSi$_2$/p-Si interfaces. Thus, in this work we showed a possible approach to change properties of the metal/semiconductor contact by varying the atomic arrangement of α-FeSi$_2$/Si heterostructure interface layer, that would be able to encourage the application of α-FeSi$_2$ phase in nanoelectronics to create easily tuneable Schottky barrier contacts, gate electrodes, local interconnects, and diffusion barriers.

REFERENCES

1. G. Shine and K. C. Saraswat, IEEE Trans. Electron Dev. **64**, 3768 (2017).
2. R. Islam, G. Shine, and K. C. Saraswat, Appl. Phys. Lett. **105** (2014).
3. V. Heine, Phys. Rev. A **138**, 1689 (1965).
4. A. Agrawal, J. Lin, M. Barth, R. White, B. Zheng, S. Chopra, S. Gupta, K. Wang, J. Gelatos, S. E. Mohney, and S. Datta, Appl. Phys. Lett. **104**, 8 (2014).
5. I. A. Tarasov, M. A. Visotin, A. S. Aleksandrovsky, N. N. Kosyrev, I. A. Yakovlev, M. S. Molokeev, A. V. Lukyanenko, A. S. Krylov, A. S. Fedorov, S. N. Varnakov, and S. G. Ovchinnikov, J. Magn. Magn. Mater. **440**, 144 (2017).
6. I. A. Tarasov, I. A. Yakovlev, M. S. Molokeev, M. Rautskii, I. V. Nemtsev, S. N. Varnakov, and S. G. Ovchinnikov, Mater. Lett. **168**, 90 (2016).
7. B.-X. Xu, Y. Zhang, H.-S. Zhu, D.-Z. Shen, and J.-L. Wu, Mater. Lett. **59**, 833 (2005).
8. B. Aronsson, D. H. Templeton, S. Rundqvist, E. Varde, and G. Westin, Acta Chem. Scand. **14**, 1414 (1960).

9. W. Miiller, J. M. Tomczak, J. W. Simonson, G. Smith, G. Kotliar, and M. C. Aronson, J. Phys.: Condens. Matter **27**, 175601 (2015).

10. J. K. Tripathi, G. Markovich, and I. Goldfarb, Appl. Phys. Lett. **102**, 251604 (2013).

11. J. K. Tripathi, M. Garbrecht, W. D. Kaplan, G. Markovich, and I. Goldfarb, Nanotechnology **23**, 495603 (2012).

12. J. K. Tripathi, R. Levy, Y. Camus, M. Dascalu, F. Cesura, R. Chalasani, A. Kohn, G. Markovich, and I. Goldfarb, Appl. Surf. Sci. **391**, 24 (2017).

13. V. S. Zhandun, N. G. Zamkova, S. G. Ovchinnikov, and I. S. Sandalov, Phys. Rev. B **95**, 54429 (2017).

14. G. Cao, D. J. Singh, X.-G. Zhang, G. Samolyuk, L. Qiao, C. Parish, K. Jin, Y. Zhang, H. Guo, S. Tang, W. Wang, J. Yi, C. Cantoni, W. Siemons, E. A. Payzant, M. Biegalski, T. Z. Ward, D. Mandrus, G. M. Stocks, and Z. Gai, Phys. Rev. Lett. **114**, 147202 (2015).

15. N. Jedrecy, A. Waldhauer, M. Sauvage-Simkin, R. Pinchaux, and Y. Zheng, Phys. Rev. B **49**, 4725 (1994).

16. J. Chevrier, P. Stocker, L. T. Vinh, J. M. Gay, and J. Derrien, Europhys. Lett. **22**, 449 (1993).

17. X. W. Lin, M. Behar, J. Desimoni, H. Bernas, J. Washburn, and Z. Liliental-Weber, Appl. Phys. Lett. **63**, 105 (1993).

18. S. S. Pan, C. Ye, X. M. Teng, H. T. Fan, and G. H. Li, Phys. Status Solidi **204**, 3316 (2007).

19. C. Detavernier, C. Lavoie, J. Jordan-Sweet, and A. S. Özcan, Phys. Rev. B **69**, 174106 (2004).

20. Y. Gao, G. Shao, R. S. Chen, Y. T. Chong, and Q. Li, Solid State Commun. **149**, 97 (2009).

21. Z.-Q. Zou, X. Li, X.-Y. Liu, K.-J. Shi, and X.-Q. Guo, Appl. Surf. Sci. **399**, 200 (2017).

22. S. Liang, R. Islam, D. J. Smith, and P. A. Bennett, J. Cryst. Growth **295**, 166 (2006).

23. D. Das, J. C. Mahato, B. Bisi, B. Satpati, and B. N. Dev, Appl. Phys. Lett. **105**, 191606 (2014).

24. V. E. Borisenko, *Semiconducting Silicides: Basics, Formation, Properties* (Springer, Berlin, Heidelberg, 2011).

25. J. Karel, J. Juraszek, J. Minar, C. Bordel, K. H. Stone, Y. N. Zhang, J. Hu, R. Q. Wu, H. Ebert, J. B. Kortright, and F. Hellman, Phys. Rev. B **91**, 144402 (2015).

26. M. N. Volochaev, I. A. Tarasov, Y. Y. Loginov, A. G. Cherkov, and I. V. Kovalev, J. Phys.: Conf. Ser. **857**, 12053 (2017).

27. S. N. Varnakov, A. A. Lepeshev, S. G. Ovchinnikov, A. S. Parshin, M. M. Korshunov, and P. Nevoral, Instrum. Exp. Tech. **47**, 839 (2004).

28. I. A. Yakovlev, S. N. Varnakov, B. A. Belyaev, S. M. Zharkov, M. S. Molokeev, I. A. Tarasov, and S. G. Ovchinnikov, JETP Lett. **99**, 527 (2014).

29. N. V. Volkov, A. S. Tarasov, D. A. Smolyakov, A. O. Gustaitsev, M. V. Rautskii, A. V. Lukyanenko, M. N. Volochaev, S. N. Varnakov, I. A. Yakovlev, and S. G. Ovchinnikov, AIP Adv. **7**, 15206 (2017).

30. L. A. Solovyov, J. Appl. Crystallogr. **37**, 743 (2004).

31. S. M. Sze, *Physics of Semiconductor Devices* (Wiley-Interscience, New York, 1969).